

Growth Mechanism of Langmuir-Blodgett Films

J. K. Basu, S. Hazra, and M. K. Sanyal

Surface Physics Division, Saha Institute of Nuclear Physics, 1/AF, Bidhannagar, Calcutta 700 064, India
(Received 23 July 1998)

Langmuir-Blodgett (LB) deposition is an astonishingly simple technique to grow well-ordered correlated metal-organic multilayers. To understand this growth mechanism, we have performed x-ray scattering and atomic force microscopic (AFM) studies on cadmium arachidate LB films exhibiting self-affine and logarithmic in-plane correlation at the interfaces. Using linear stochastic theory for interface evolution, it is proposed that a 1D deposition followed by a 2D desorption process is the growth mechanism of LB films. X-ray and AFM measurements confirm the crossover between these two growth regimes. [S0031-9007(99)09320-5]

PACS numbers: 68.18.+p, 68.10.-m, 68.55.-a, 81.10.Aj

Metal-organic films deposited by the Langmuir-Blodgett (LB) technique have been the subject of intense research due to their ease of preparation, potential applications in various fields [1–4], and availability of sophisticated structural characterization techniques, such as atomic force microscopy (AFM) and x-ray–neutron reflectometry. X-ray scattering studies had shown that the interfacial correlation of these films can vary from self-affine fractal [5,6], observed in diverse physical systems [7], to long range logarithmic [8], characteristic of capillary waves on liquid surfaces [9]. It is expected that systematic studies of these interfacial morphology can provide us a clue to the growth mechanism of LB films, especially because a lot of theoretical and simulation studies have been performed to link the evolution of the interfacial morphology with the possible growth mechanism of thin films [7,10].

We have performed x-ray scattering and AFM studies on LB films of cadmium arachidate (CdA) deposited on silicon and quartz substrates. X-ray specular and longitudinal scans were performed by keeping the incident angle (θ_i) and the detector angle (θ_d) equal and at a fixed offset (0.12° here), respectively; on the other hand, transverse scans were taken with the fixed scattering angle ($\theta_i + \theta_d$) by rotating the sample. Collected transverse data are shown in Fig. 1 and the specular and longitudinal data are shown in Fig. 2. The transverse data of films deposited on silicon and quartz exhibit peak shapes which are characteristic of self-affine [5,10] and logarithmic [8,9] interfacial correlation, respectively. For the present study, LB films of CdA, each nine monolayers, were prepared in a trough (KSV instruments) using the standard process [1,2] from the Langmuir monolayer of arachidic acid kept at the fixed pressure of 30 mN m^{-1} on the cadmium chloride solution maintained at a temperature of 10°C and $p\text{H}$ of 6.5. This process involves repeated up-down movements of a vertical substrate from water to air [(a) \rightarrow (b) \rightarrow (c)] and vice versa [(c) \rightarrow (b) \rightarrow (a)] through this monolayer [refer to Fig. 2(A)] at a fixed rate (3 mm min^{-1} here). A drying time is given between the up and down cycle (10 min in our case). Molecules are transferred to the substrate at the air-water-substrate contact line, a one-

dimensional (1D) interface, and considerable molecular rearrangement can take place during this transfer [position (b) in Fig. 2(A)] [11]. These transferred molecules form a two-dimensional (2D) layer [3,11,12] on the substrate with

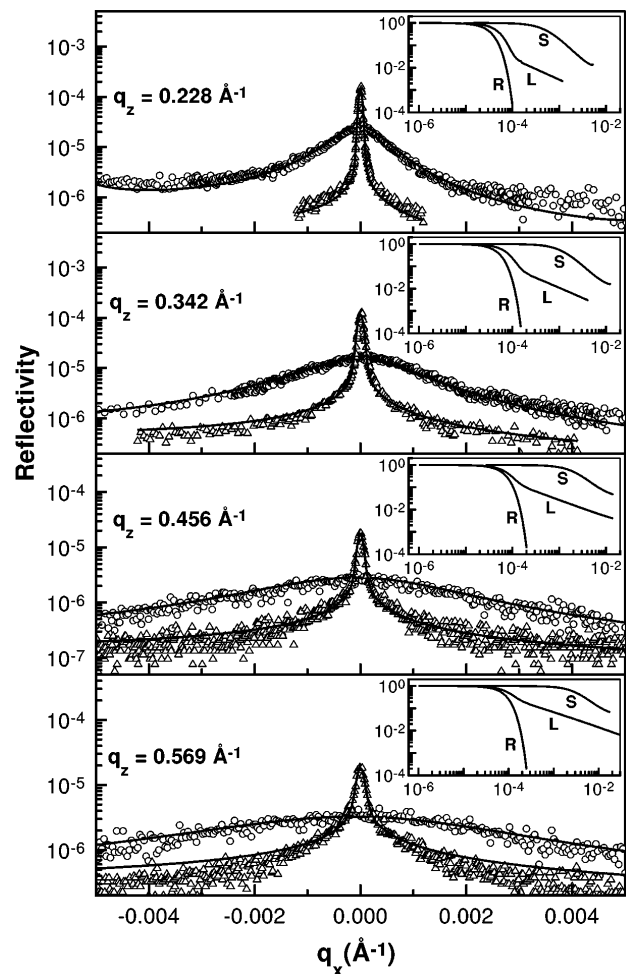


FIG. 1. Transverse diffuse scattering data at four multilayer Bragg peak positions (indicated by the q_z values) for the LB films. The data for films on silicon (\circ) and quartz (\triangle) are shown along with the calculated profiles (solid lines). In the insets the functions \mathcal{F}_S , \mathcal{F}_L , and \mathcal{R} (indicated by S, L, and R) are plotted against q_x in the log-log scale.

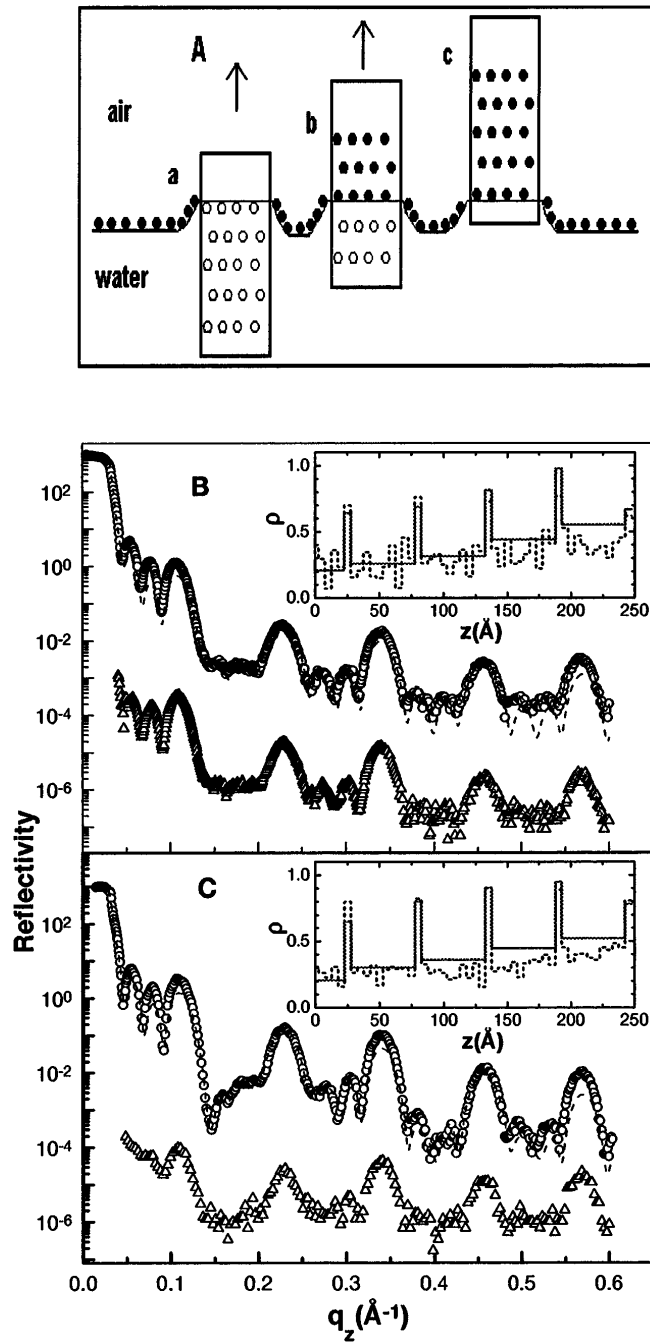


FIG. 2. (A) Schematic diagram of the LB deposition process is shown by indicating three distinct positions of the film, namely, (a) in water, (b) in the air-water-substrate contact line, where the actual transfer of molecules (indicated by solid circles) takes place, and (c) in air. Open circles in the substrate indicate previously transferred molecules or expected cites. (B) shows the specular reflectivity data (\circ), detailed (solid line), and simple (dashed line) model fit for the LB film on silicon. Also shown are the longitudinal data (\triangle) and fit (solid line). Specular data and fit are shifted up for clarity. The inset shows the obtained detailed (dashed line) and simple (solid line) electron density as a function of depth, z , from the top of the film. (C) shows the same set, as in (B), for the film on quartz.

previously transferred molecules, and this 2D layer settles through a desorption process during drying time and during the time when the film is immersed in water [positions (c) and (a), respectively, in Fig. 2(A)].

To explain the growth of LB films we have used here a general linear stochastic equation [7] for the interface evolution of solid films,

$$\frac{\partial h}{\partial t} = \nu \nabla^2 h - \Lambda \nabla^4 h + N_d + N. \quad (1)$$

Here h denotes the height above a mean reference surface and t denotes time. The first and second terms in the right-hand side of the equation describe the adsorption/desorption process controlled by the surface tension and the diffusion process, respectively [7]. ν and Λ are constants related to the corresponding surface tension and diffusion, respectively. N_d is conservative diffusive noise arising due to surface diffusion with $\langle N_d \rangle = 0$; N , on the other hand, is nonconservative deposition noise so that $\langle N \rangle \neq 0$, over the entire surface. For any growth process that involves diffusion followed by adsorption/desorption, a length scale $\xi (\sim \sqrt{\Lambda/\nu})$ can be defined below which the exponents of the growth process α and β are decided predominantly by diffusion. These exponents are a measure of the interfacial width σ of the system and can be defined in terms of the following scaling relations as $\sigma \sim r^\alpha$ as $t \rightarrow \infty$, where r is the measured length scale, and $\sigma \sim t^\beta$ as $t \rightarrow 0$.

In our growth model we further assumed that the diffusion process is occurring predominantly at the 1D interface, referred to earlier, and in this process the dominating noise is N_d . As a result the second and third terms are the dominant terms in deciding the scaling behavior of the system and α, β can be written as $(2-d)/2$ and $(2-d)/8$ [7], respectively, with the dimension $d = 1$ here. On the other hand, during the 2D adsorption/desorption process N dominates because of the loss of molecules so that in Eq. (1) above the first and fourth terms dominate in deciding scaling behavior of the system and α, β becomes $(2-d)/2$ and $(2-d)/4$, respectively (here $d = 2$) [7]. So a crossover ($\alpha = 1/2 \rightarrow 0; \beta = 1/8 \rightarrow 0$) to a slow logarithmic growth of the Edwards-Wilkinson-type [13] occurs above ξ . Although on the basis of the measured saturated roughness exponent α , other 1D transfer processes [7] having the same α cannot be ruled out here, the basic nature of our growth model remains valid. This model has given us a unified height difference correlation function, $g(r)$, for the LB films and is consistent with the measured α and ξ .

The correlation function, $g(r)$ (above a lower cutoff of about molecular diameter) for conformal interfaces can be written as

$$\begin{aligned} g(r) &= \langle [h(0) - h(r)]^2 \rangle \\ &= \left\{ 2\sigma_0^2 + B \left[\gamma_E + \ln \left(\frac{\kappa r}{2} \right) \right] \right\} \{ 1 - \exp[-(r/\xi)^{2\alpha}] \}. \end{aligned} \quad (2)$$

Here σ_0 is the *true* rms roughness, γ_E is the Euler constant, and κ is a lower cutoff wave vector ($\sim 10^{-5} \text{ \AA}^{-1}$ here) for logarithmic correlation, $B = k_B T / \pi \gamma$ and γ is the interfacial tension [8,9]. X-ray scattering probes this correlation function and depending on the relative magnitude of the x-ray coherence length, ζ ($\approx 10 \mu\text{m}$ here), and correlation length, ξ , one of the terms in this correlation function will dominate. If $\xi \ll \zeta$, the first term in Eq. (2) is dominant and hence the interface exhibits logarithmic correlation as was observed earlier [8]. In another extreme, for $\xi \gg \zeta$, the second term in Eq. (2) dominates and $g(r)$ is found to scale in a self-affine manner without *cutoff* ζ , as $g(r) = Ar^{2\alpha}$. In the intermediate region ($\xi < \zeta$) $g(r)$ takes the standard form [10] and the value of ξ can be extracted from x-ray scattering measurements [6,14].

X-ray measurements were performed with a rotating anode Cu $K_{\alpha 1}$ source [8] with a scattering geometry that effectively integrates out the component of scattering in the q_y direction. After convolution of the Gaussian resolution function, $\mathcal{R}(q_x)$, with the scattering cross section one obtains the total scattered intensity, $I(q_x, q_z)$, in the q_x - q_z scattering plane, for a multilayered system with conformal rough interfaces as

$$I(q_x, q_z) = I_0 \frac{R_P(q_z) q_z}{2k_0 \sin \theta_i} \mathcal{G}(q_z) \mathcal{F}(q_x, q_z) + D. \quad (3)$$

Here $R_P(q_z)$ is the reflectivity for a multilayer with sharp interfaces calculated using the Parratt technique [15], $k_0 = 2\pi/\lambda$, I_0 is the direct beam intensity, and D ($= 0.04$ counts/sec) is a constant background arising, mainly, due to the detector dark current. q_x and q_z are the transverse and longitudinal wave vectors, respectively, and $\mathcal{G}(q_z)$ and $\mathcal{F}(q_x, q_z)$ are functions which depend on the form of the height difference correlation function, as explained below.

For a system with self-affine rough interfaces with $\alpha = 0.5$, as observed here and earlier [5], one obtains the Lorentzian shaped transverse diffuse profile, $I(q_x)$ with fixed q_z , and the width of this profile scales as q_z^2 [5,10]. By using subscript S we can express $I(q_x, q_z)$, in terms of the two functions defined below as

$$\mathcal{G}_S(q_z) = q_z^3 I_{\text{conv}}(q_x, q_z)_{q_x=0}, \quad (4a)$$

$$\mathcal{F}_S(q_x, q_z) = I_{\text{conv}}(q_x, q_z) / I_{\text{conv}}(q_x, q_z)_{q_x=0}. \quad (4b)$$

Here $I_{\text{conv}}(q_x, q_z)$ is a resolution convoluted Lorentzian function,

$$I_{\text{conv}}(q_x, q_z) = \left[\frac{A}{q_{xc}^2 + \left[\frac{A}{2} q_z^2 \right]^2} \right] \otimes \mathcal{R}(q_x), \quad (5)$$

where $A \approx 2\sigma_0^2/\xi$ (neglecting slow logarithmic variation).

In the case of logarithmic rough interfaces diffuse scattering has an asymptotic tail (as a function of q_x) with an exponent that increases with q_z along with diffuse to specular ratio [8,9]. A subscript L has been used to

represent $I(q_x, q_z)$ in terms of the two functions defined below as

$$\mathcal{G}_L(q_z) = \exp(-q_z^2 \sigma_{\text{eff}}^2) \frac{1}{\sqrt{\pi}} \Gamma\left(\frac{1-\eta}{2}\right), \quad (6a)$$

$$\mathcal{F}_L(q_x, q_z) = {}_1F_1\left(\frac{1-\eta}{2}; \frac{1}{2}; \frac{-q_x^2 \xi^2}{4\pi^2}\right), \quad (6b)$$

where ${}_1F_1$ is the Kummer function, $\eta = Bq_z^2/2$, and σ_{eff} is the effective interface roughness [10,11]. The functions, \mathcal{F}_S and \mathcal{F}_L , reduce to unity at $q_x = 0$ (specular condition).

Equations (3) and (4) represent well (Fig. 1) the transverse diffuse profiles for the film on silicon and the only fit parameter A comes out to be $0.02 \pm 0.002 \text{ \AA}$. Equations (3) and (6) fit very well all the profiles of the film on quartz with $B = 2.1 \pm 0.1 \text{ \AA}^2$, $\sigma_{\text{eff}} = 2.5 \pm 0.1 \text{ \AA}$, respectively. The difference in the scaling of the widths and the specular to diffuse intensity ratio for the two profiles \mathcal{F}_S and \mathcal{F}_L , as functions of q_z , are clearly evident in the insets of Fig. 1.

In Fig. 2 it can be seen that the longitudinal data follow the specular data closely, confirming that interfaces are conformal. The electron density profiles (EDP) obtained for the films on silicon and quartz are shown in the insets of Fig. 2. Higher electron density of the metallic layer just above the substrate for the film on quartz produces a dip ($q_z = 0.12 \text{ \AA}^{-1}$) in the reflectivity profile and increases intensity of the x-ray multilayer peaks. For both the films the total thickness and average bilayer spacing came out to be 247.5 \AA and 55 \AA , respectively, indicating stacking of untilted molecules in these deposited films. Although the essential features of the specular data, for both the films, are obtained using the simple model (ten slices), the reflectivity profiles obtained using the detailed model EDP, with slices of 5 \AA (50 slices), matches with the data almost exactly.

AFM (Autoprobe CP, Park Scientific) images of LB films were collected in a constant force contact mode using a silicon nitride tip in ambient condition with a $100 \mu\text{m}$ scanner. Two such images of the films are shown in Fig. 3. The rms roughness (σ) obtained from the average of several scans of a particular scan size is plotted as a function of the scan length for both the films in Fig. 4. It can be readily observed that the roughness of the film on silicon increases considerably with the scan size up to a certain *cutoff* length scale $\sim 15 \mu\text{m}$ and after that it gets saturated to $\sim 25 \text{ \AA}$ the molecular length. This *cutoff* length scale is the same [7,16] in-plane correlation length, ξ , which is larger than the x-ray coherence length here. Below ξ , the variation of σ of the film on silicon follows $\sigma \sim r^\alpha$ with exponent $\alpha \sim 0.5$, as obtained from the linear fit and confirms x-ray results. The variation of σ^2 of the film on quartz is slow and follows a logarithmic relation as observed in x-ray data. From the slope of the linear fit obtained in the semilog plot one can calculate the surface tension, γ [refer to Eq. (2)]. The value of γ comes

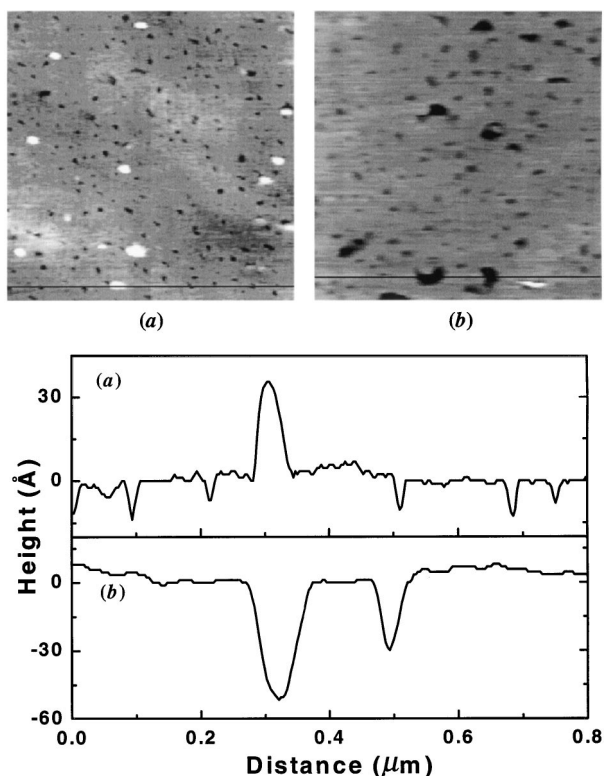


FIG. 3. AFM images of scan size $0.8 \mu\text{m} \times 0.8 \mu\text{m}$ for the LB films on (a) silicon and (b) quartz. Typical line profiles drawn through each image are shown at the bottom of the figure.

out to be $\sim 7 \text{ mN m}^{-1}$, which is quite small compared to the value of $\sim 63 \text{ mN m}^{-1}$ estimated from the fit to the x-ray data. This difference arises probably due to the different surface tensions of the amphiphilic tails at the top surface, as measured by AFM, and that of the metal ions in buried interfaces, which contribute predominantly to x-ray scattering.

It is also to be noted from the images that both the films contain lots of defects of different size and height. The typical size and height of the defects can be observed by drawing line profiles (refer to Fig. 3). Large sized ($\sim 700 \text{ \AA}$ wide and $\sim 55 \text{ \AA}$ deep) craters could be seen in the film deposited on quartz. This may be a signature of the 2D desorption process. On the other hand, strong fluctuations around the mean surface were observed for the film deposited on silicon. This may be a signature of domains but without well-defined size. As a result, like previous attempts [14] even with better resolution, we could not detect the signature of monodispersed domains, which would have led to the reduction of the width of transverse profiles as a function of q_z .

In conclusion we have obtained a unified height-height correlation function that explains observed morphology of LB films and demonstrates clearly the link between this correlation function and growth mechanism that involves 1D diffusion and 2D adsorption. A *cutoff* length

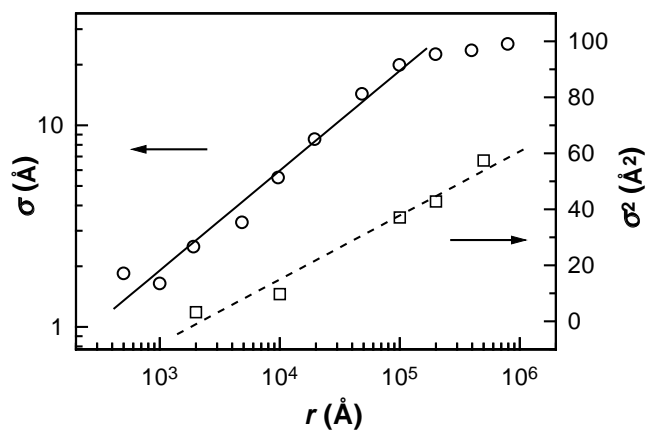


FIG. 4. Variation of roughness (σ) with scan length for the LB films. $\log \sigma$ vs $\log r$ for the film on silicon (\circ). Solid line is the linear fit to the data below $\xi \sim 15 \mu\text{m}$. σ^2 vs $\log r$ for the film on quartz (\square). Dashed line is the linear fit to the data.

arises from the interplay of these two processes and the maximum value of this length can be large and is dictated by the length of the molecules being deposited. To our knowledge, these real and reciprocal space AFM and x-ray measurement techniques have not been used earlier to understand the growth mechanism of fractal surface morphology seen in many diverse physical systems of general interest.

- [1] *Langmuir-Blodgett Films*, edited by G. Roberts (Plenum, New York, 1990).
- [2] A. Ulman, *Introduction to Ultrathin Organic Films* (Academic, New York, 1991).
- [3] D.K. Schwartz, *Surf. Sci. Rep.* **27**, 241 (1997).
- [4] R. Tollner *et al.*, *Science* **278**, 2100 (1997); C.P. Collier *et al.*, *Science* **277**, 1978 (1997); A.V. Bune *et al.*, *Nature (London)* **391**, 874 (1998).
- [5] A. Gibaud *et al.*, *Phys. Rev. Lett.* **74**, 3205 (1995).
- [6] V. Nitz *et al.*, *Phys. Rev. B* **54**, 5038 (1996).
- [7] A.-L. Barabasi and H.E. Stanley, *Fractal Concepts in Surface Growth* (Cambridge University Press, New York, 1995); P. Meakin, *Phys. Rep.* **235**, 189 (1993); J. Krug, *Adv. Phys.* **46**, 139 (1997).
- [8] J.K. Basu and M.K. Sanyal, *Phys. Rev. Lett.* **79**, 4617 (1997).
- [9] M.K. Sanyal *et al.*, *Phys. Rev. Lett.* **66**, 628 (1991).
- [10] S.K. Sinha *et al.*, *Phys. Rev. B* **38**, 2297 (1988).
- [11] J.E. Riegler and J.D. LeGrange, *Phys. Rev. Lett.* **61**, 2492 (1988); A. Leuthe and H. Riegler, *J. Phys. D* **25**, 1766 (1992).
- [12] A. Malik *et al.*, *Phys. Rev. B* **52**, 11 654 (1995).
- [13] S.F. Edwards and D.R. Wilkinson, *Proc. R. Soc. London A* **381**, 17 (1982).
- [14] U. Englisch *et al.*, *Physica (Amsterdam)* **248B**, 258 (1998).
- [15] L.G. Parratt, *Phys. Rev.* **95**, 359 (1954).
- [16] L. Vazquez *et al.*, *Phys. Rev. Lett.* **79**, 709 (1997).